Electronic Supplementary Material

Dealloyed TiCuMn efficiently catalyze the NO reduction and Zn-NO batteries

Lang Zhang[1], Tong Hou[1], Weijia Liu[1],Yeyu Wu **(✉)**[2], Tianran Wei[1], Junyang Ding **(✉)**[3], Qian Liu[4], Jun Luo[5], Xijun Liu **(✉)**[1]

1 State Key Laboratory of Featured Metal Materials and Life-Cycle Safety for Composite Structures, MOE Key Laboratory of New Processing Technology for Nonferrous Metals and Materials, School of Resources, Environment and Materials, Guangxi University, Nanning 530004, China

2 Education Department of Guangxi Zhuang Autonomous Region, Key Laboratory of Applied Analytical Chemistry, Guangxi Collaborative Innovation Center for Chemistry and Engineering of Forest Products, Guangxi Key Laboratory of Chemistry and Engineering of Forest Products, Key Laboratory of Chemistry and Engineering of Forest Products, State Ethnic Affairs Commission, School of Chemistry and Chemical Engineering, Guangxi Minzu University, Nanning 530006, China

3 Institute for New Energy Materials & Low-Carbon Technologies, School of Materials Science and Engineering, Tianjin University of Technology, Tianjin 300384, China

4 Institute for Advanced Study, Chengdu University, Chengdu 610106, China

5 ShenSi Lab, Shenzhen Institute for Advanced Study, University of Electronic Science and Technology of China, Shenzhen 518110, China

E-mails: eveyeyu@163.com (Wu Y); junyangdingde18@163.com (Ding J); xjliu@gxu.edu.cn (Liu X)

Figures and Table

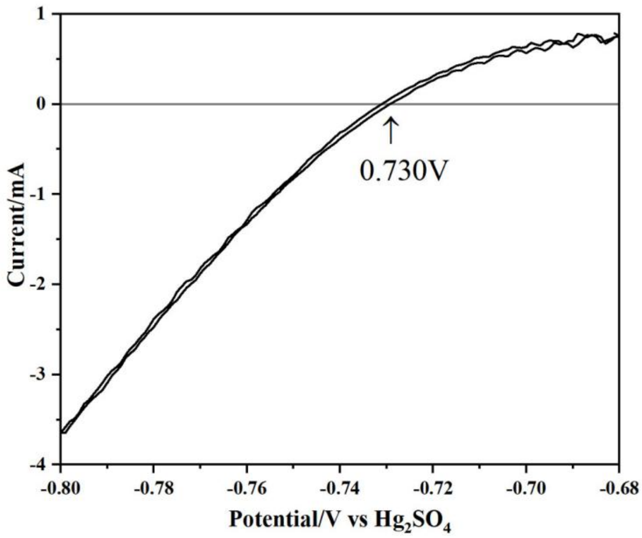

Fig. S1 The calibration CVs graph of Hg_2SO_4 electrode vs RHE.

In this work, the high purity hydrogen saturated 0.05 M H_2SO_4 as electrolyte, the Hg_2SO_4 electrode as the reference electrode, two Pt sheets (1.0 × 1.0 cm^2) as working electrode and counter electrode, respectively. As shown in Figure S1, the CVs test with a scan rate of 1 mV s^{-1} is performed and the average of the two potentials at current crossed zero is the correction potential of hydrogen electrode reactions. So in alkaline seawater, $E_{RHE} = E_{Hg2SO4} + 0.730$ V.

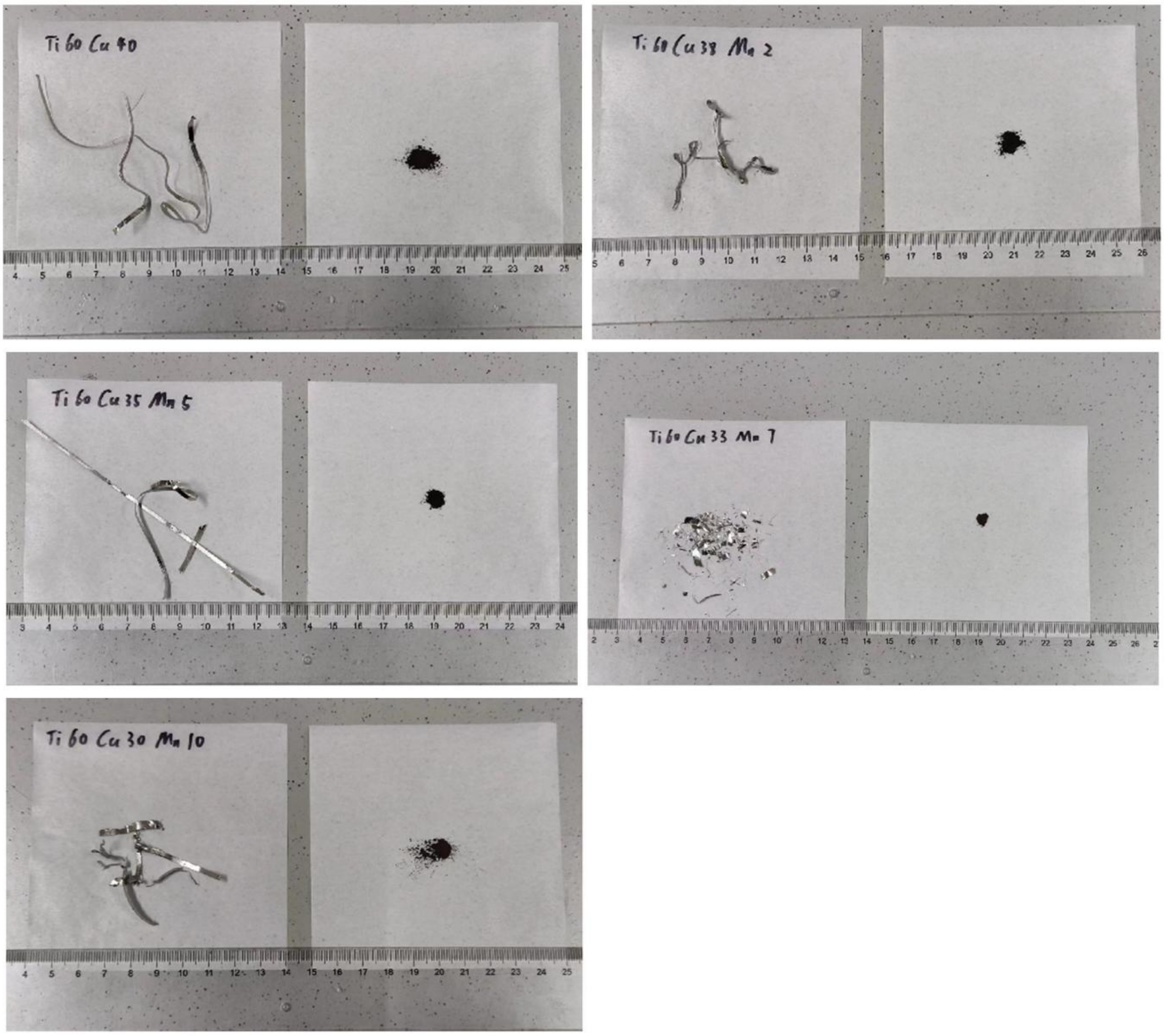

Fig. S2 The optical photographs of the d–TiCuMn based samples (a) before and (b) after dealloying treatment.

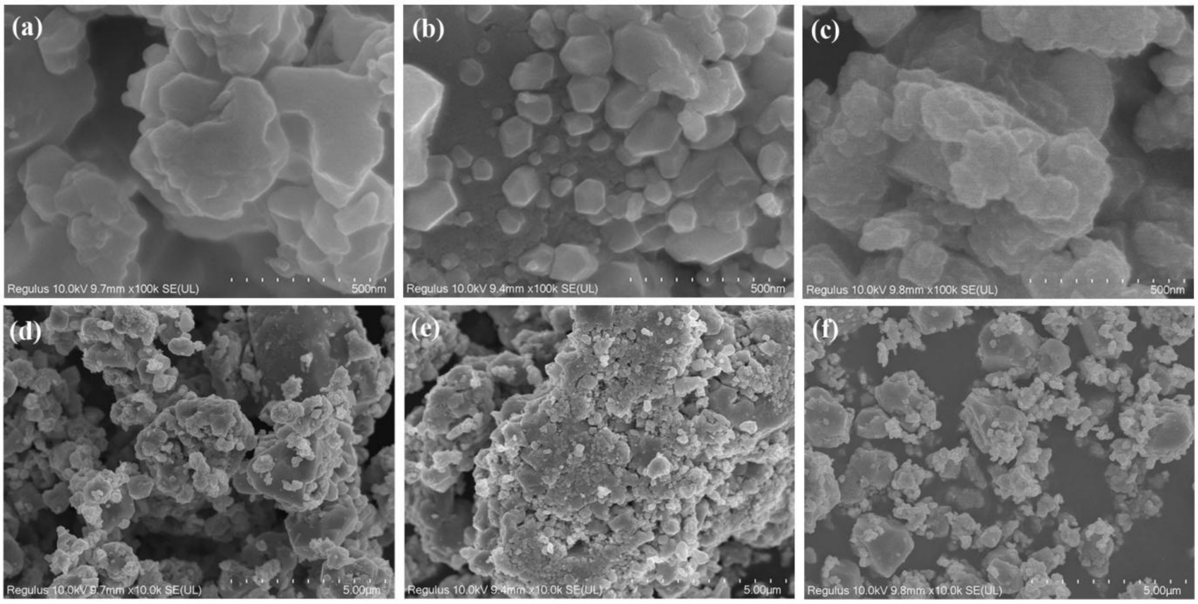

Fig. S3 SEM images of the d–TiCuMn based samples. (a,d) d–$TiCuMn_2O_x$, (b, e) d–$TiCuMn_5O_x$, and (c, f) d–$TiCuMn_{10}O_x$.

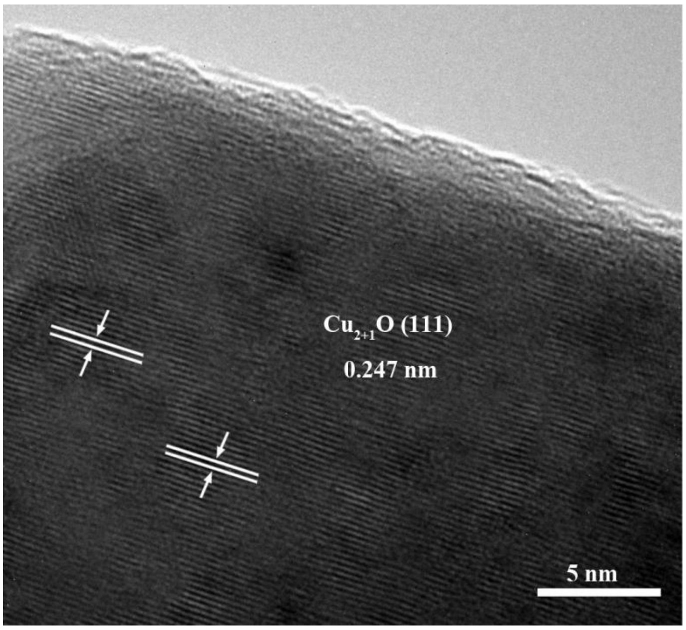

Fig. S4 HRTEM images of the d–$TiCuMn_7O_x$.

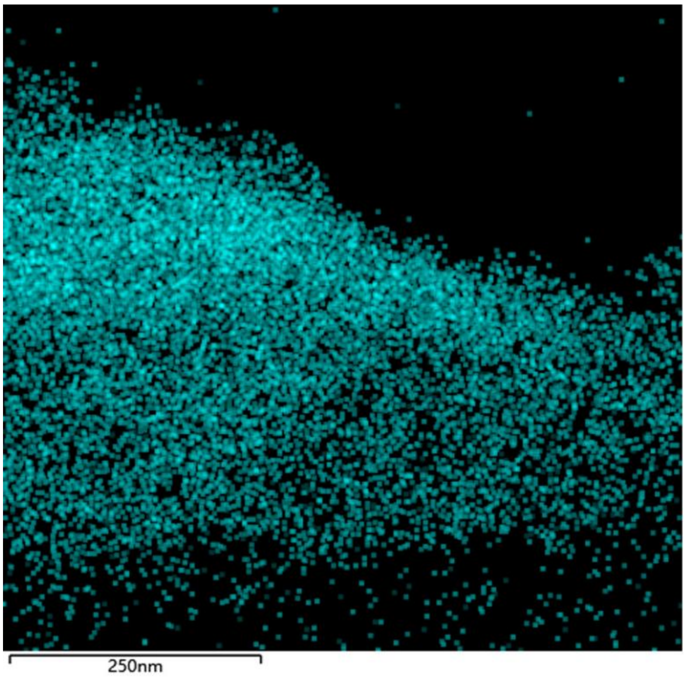

Fig. S5 EDX elemental of oxygen mapping images of d–$TiCuMn_7O_x$.

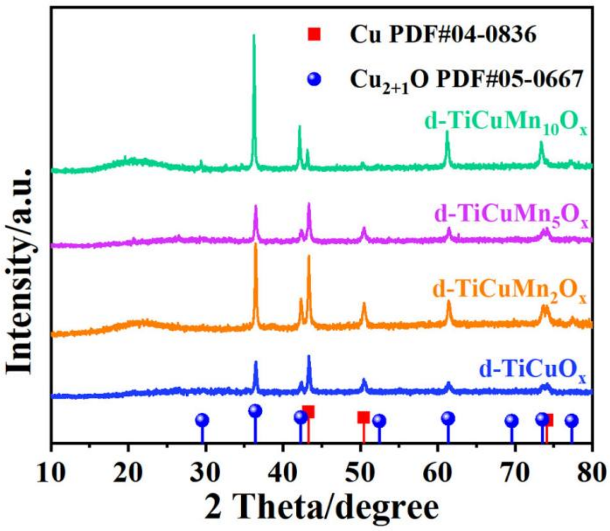

Fig. S6 XRD pattern of the d–TiCuMn based samples.

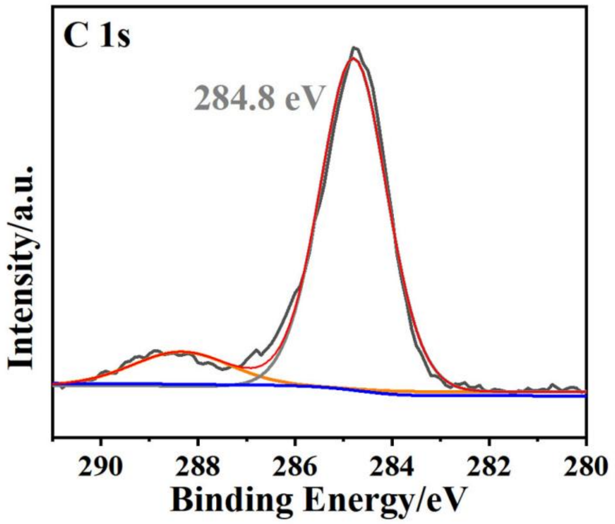

Fig. S7 High–resolution XPS spectra of C 1s for d–TiCuMn_7O_x.

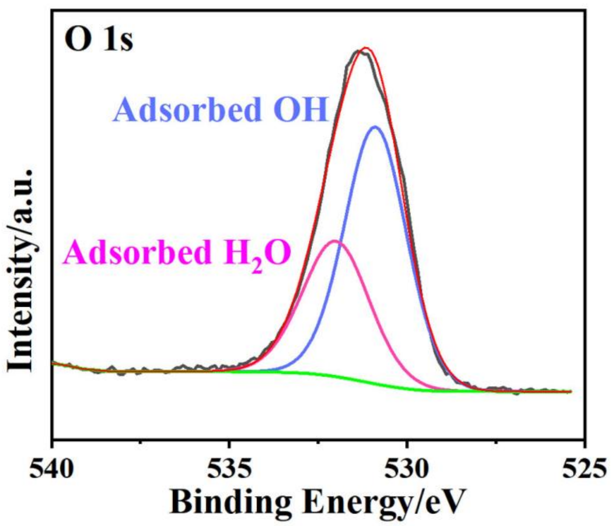

Fig. S8 High–resolution XPS spectra of O 1s for d–TiCuMn_7O_x.

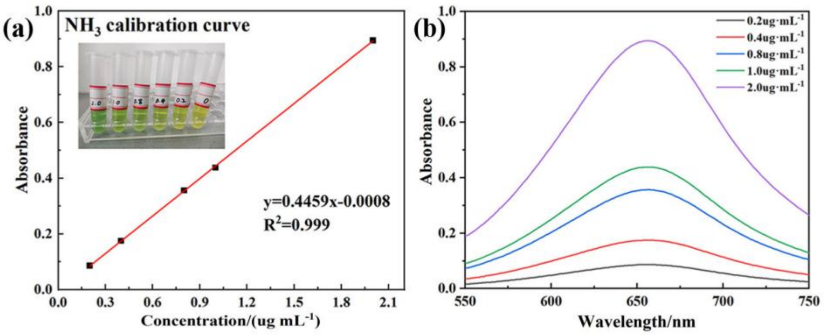

Fig. S9 (a) Calibration curve of NH_3. (b) UV–Vis absorption spectra of indophenol assays with NH_3 after incubated for 2 h at room temperature.

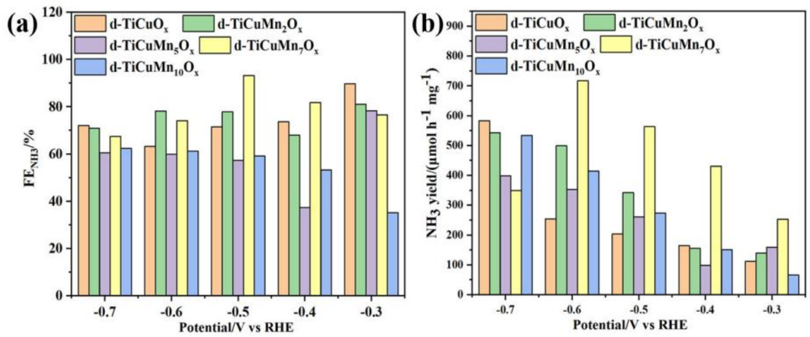

Fig. S10 (a) FE_{NH3} (b) NH_3 yield for d–TiCuMn based materials under the various applied potential.

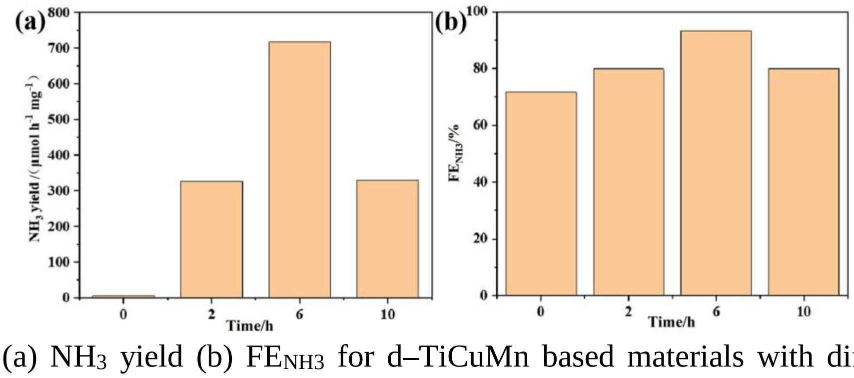

Fig. S11 (a) NH_3 yield (b) FE_{NH3} for d–TiCuMn based materials with different dealloying time.

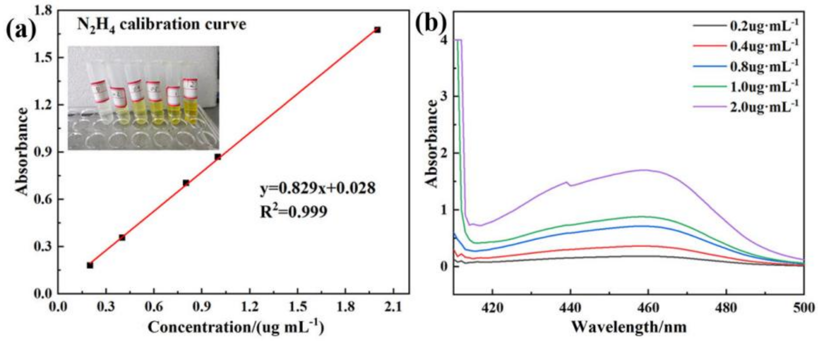

Fig. S12 (a) Calibration curve of N_2H_4. (b) UV–Vis absorption spectra of with N_2H_4 after incubated for 15 min at room temperature.

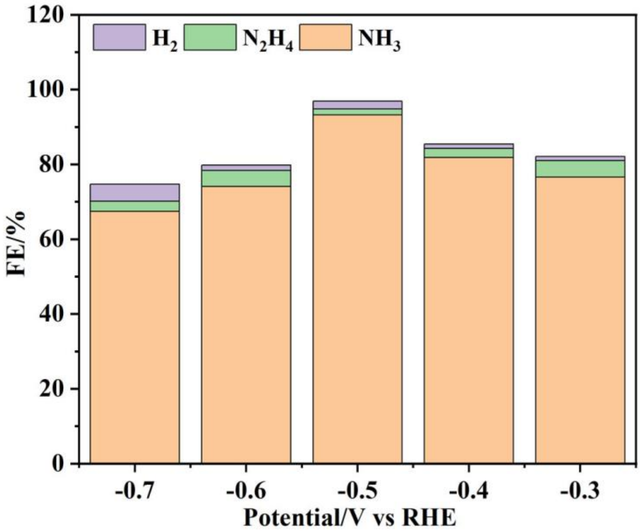

Fig. S13 FE of NH_3, H_2, and N_2H_4 for d–$TiCuMn_7O_x$ under the various applied potential.

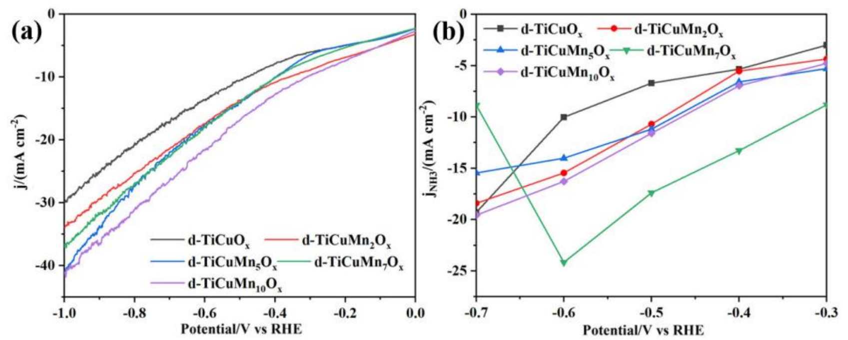

Fig. S14 (a) LSV curves and (b) NH_3 partial current densities of d–TiCuMn based materials.

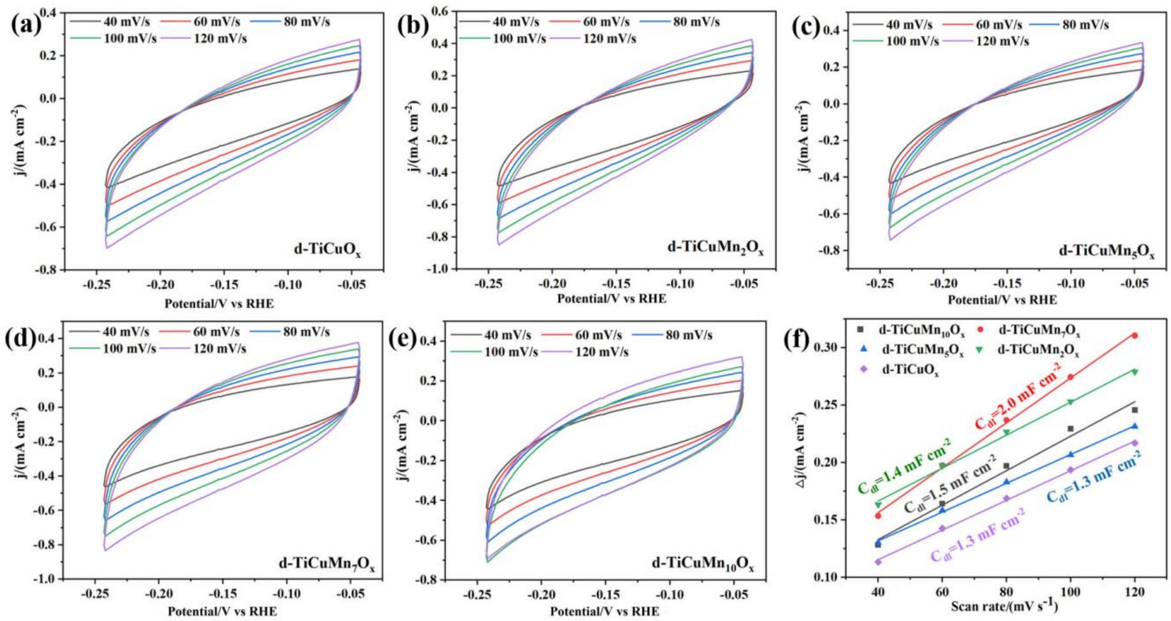

Fig. S15 (a–e) CV plots of the d–TiCuMn based samples in the region of –0.04 ~–0.24 V vs RHE. (f) The calculated double–layer capacitances of d–TiCuMn based samples.

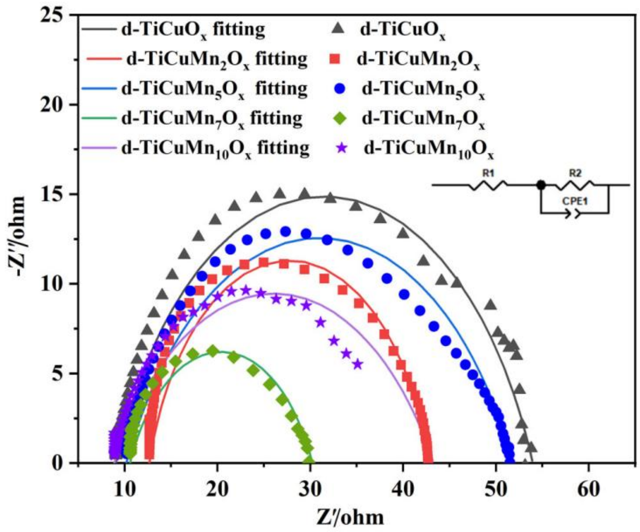

Fig. S16 Nyquist diagrams of the d–TiCuMn based materials.

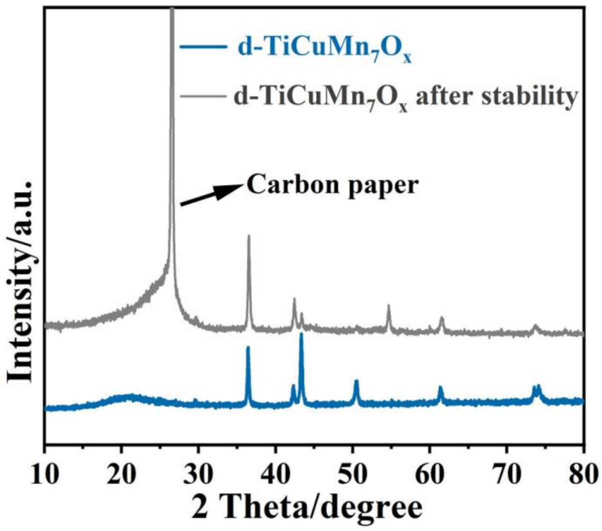

Fig. S17 XRD patterns of d–$TiCuMn_7O_x$ after 9 h stability test.

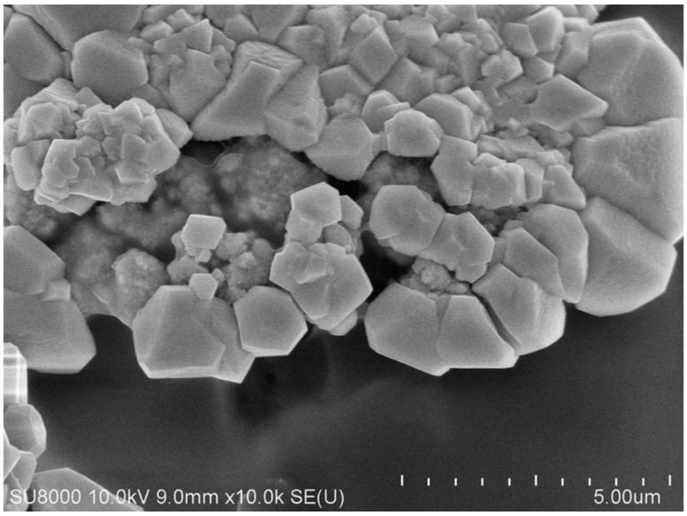

Fig. S18 SEM image of d–$TiCuMn_7O_x$ after 9 h stability test.

Table S1 Comparison of R_{ct} values obtained from equivalent electrical circuit of d–$TiCuMn_7O_x$ and control samples.

Catalysts	d–$TiCuO_x$	d–$TiCuMn_2O_x$	d–$TiCuMn_5O_x$	d–$TiCuMn_7O_x$	d–$TiCuMn_{10}O_x$
R_s/Ω	9.1	10.4	10.2	9.6	8.9
R_{ct}/Ω	46.9	36.5	42.4	24.7	39.6

Note that the solution resistance (R_s) and charge transfer resistance (R_{ct}).

Table S2 Electrocatalysis results from this work and other reported NORR results of the literature.

Catalysts	Electrolyte	Potential/V vs RHE)	FE_{NH3}/%	NH_3 yield	Reference
Co_1/MoS_2	0.5 M Na_2SO_4	–0.5	87.7	217.6 μmol h^{-1} cm^{-2}	[1]
Fe_1/MoS_{2-x}	0.5 M Na_2SO_4	–0.6	82.5	288.2 μmol h^{-1} cm^{-2}	[2]
MoS_2/GF	0.1 M HCl	0.1	76.6	99.6 μmol h^{-1} cm^{-2}	[3]
Cu_1/MoS_2	0.5 M Na_2SO_4	–0.6	90.6	337.5 μmol h^{-1} cm^{-2}	[4]
TiS_2	0.5 M Na_2SO_4	–0.6	91.6	153.8 μmol h^{-1} cm^{-2}	[5]
Mo_2C	0.5 M Na_2SO_4	–0.4	86.3	122.7 μmol h^{-1} cm^{-2}	[6]
In_1/a–MoO_3	0.5 M Na_2SO_4	–0.6	92.8	242.6 μmol h^{-1} cm^{-2}	[7]
HCP-Co	0.1 M Na_2SO_4	–0.6	72.58	439.5 μmol h^{-1} cm^{-2}	[8]
W_1/MoO_{3-x}	0.5 M Na_2SO_4	–0.5	91.2	308.6 μmol h^{-1} cm^{-2}	[9]
CoS_{1-x}/CP	0.2 M Na_2SO_4	–0.4	53.62	44.7 μmol h^{-1} cm^{-2}	[10]
Bi NDs/CP	0.1 M Na_2SO_4 + 0.05 mM Fe(II)EDTA	–0.5	89.2	1194.0 μg h^{-1} mg^{-2}	[11]
Cu/P–TiO_2	0.1 M K_2SO_4	–0.6	86.49	3520.8 μg h^{-1} mg^{-2}	[12]
d–$TiCuMn_7O_x$	0.05 M H_2SO_4	–0.6	74.1	717.4 μmol h^{-1} mg^{-2}	This work
d–$TiCuMn_7O_x$	0.05 M H_2SO_4	–0.5	93.2	564.3 μmol h^{-1} mg^{-2}	This work

Reference

[1] Xiaotian Li, Kai Chen, Xubin Lu, Dongwei Ma, Ke Chu. Chemical Engineering Journal 454 (2023) 140333.

[2] Kai Chen, Jiaxin Wang, Jilong Kang, Xubin Lu, Xiaolin Zhao, Ke Chu. Applied Catalysis B: Environmental 324 (2023) 122241.

[3] Longcheng Zhang, Jie Liang, YuanyuanWang, Ting Mou, Yiting Lin, Luchao Yue,

Tingshuai Li, Qian Liu, Yonglan Luo, Na Li, Bo Tang, Yang Liu, Shuyan Gao, Abdulmohsen Ali Alshehri, Xiaodong Guo, Dongwei Ma, and Xuping Sun. Angew. Chem. Int. Ed. 2021, 60, 25263-25268.

[4] Kai Chen, Guike Zhang, Xiaotian Li, Xiaolin Zhao and Ke Chu. ISSN 1998-0124 CN 11-5974/O4.

[5] Xiangli Wang, Lan Yang, Guike Zhang and Ke Chu. New J. Chem., 2023, 47, 17769.

[6] Kai Chen, Peng Shen, Nana Zhang, Dongwei Ma and Ke Chu. Inorg. Chem. 2023, 62, 653-658.

[7] Kai Chen, Nana Zhang, Fuzhou Wang, Jilong Kang and Ke Chu. J. Mater. Chem. A, 2023, 11, 6814.

[8] Dongdong Wang, ZhiWen Chen, Kaizhi Gu, Chen Chen, Yingying Liu, Xiaoxiao Wei, Chandra Veer Singh and Shuangyin Wang. J. Am. Chem. Soc. 2023, 145, 6899-6904.

[9] Kai Chen, Jiaxin Wang, Hu Zhang, Dongwei Ma and Ke Chu. Nano Lett. 2023, 23, 1735-1742.

[10] Longcheng Zhang, Qiang Zhou, Jie Liang, Luchao Yue, Tingshuai Li, Yongsong Luo, Qian Liu, Na Li, Bo Tang, Feng Gong, Xiaodong Guo and Xuping Sun. Inorg. Chem. 2022, 61, 8096-8102.

[11] Yiting Lin, Jie Liang, Haobo Li, Longcheng Zhang, Ting Mou, Tingshuai Li, Luchao Yue, Yuyao Ji, Qian Liu, Yonglan Luo, Na Li, Bo Tang, Qi Wu, Mohamed S. Hamdy, Dongwei Ma, Xuping Sun. Materials Today Physics 22 (2022) 100611.

[12] Lei Chen, Wenting Sun, Zhiying Xu, Minghui Hao, Baojing Li, Xin Liu, Jingjing Ma, Liang Wang, Chunhu Li, Wentai Wang. Ceramics International 48 (2022) 21151-21161.